conclusion[43] that there would be no macrocyclic enthalpy in the gas phase seems unlikely in the face of the fact that studies of several metal ions in the gas phase have shown[16-18] that there is a strong increase in enthalpy of complex formation as the nitrogen donor changes from primary to secondary, as shown in Figure 4. In addition, the relation between ΔH of complex formation and ligand field strength in polyamine complexes of Cu(II) and Ni(II) demonstrated by Fabbrizzi, Paoletti, and Lever[44] suggests that it is unlikely that a strong increase in LF strength as found for macrocyclic complexes compared with their open chain analogues would not be accompanied by a related increase in ΔH.

Conclusions

The data presented here appear to support the following conclusions.

(1) The increased ligand field strength found in complexes of macrocyclic ligands is at a maximum in the macrocycles which fit with the least steric strain around the metal ions.

(2) The increased LF strength is caused by the inductive effect of the increased number of secondary nitrogen donors present in a low-strain situation, which also contributes to the macrocyclic enthalpy.

(3) An important contribution to the macrocyclic enthalpy comes from strain in the cavity of the macrocycle, which in the gas phase would be caused by dipole–dipole repulsion and in aqueous solution would have a contribution from steric hindrance to solvation.

(4) van der Waals repulsions between ligands mean that for most metal ions the observed M–N bond lengths are somewhat longer than the strain-free lengths. This effect is of paramount importance for Co(III), which has a very short ideal Co–N length of 1.925 Å, which length is not realized in many of its complexes because of van der Waals repulsions. Only in complexes such as its complex with 13-aneN_4 can the ideal bond length be realized, and here we see a remarkably high LF.

Acknowledgment. We thank the Senate Research Grants Committee of the University of the Witwatersrand and the Council for Scientific and Industrial Research for generous financial support and a bursary to V.J.T.

Registry No. $[Co(NH_3)_6]^{3+}$, 28219-81-0; $[Co(en)_3]^{2+}$, 23523-25-3; $[Co(pn)_3]^{2+}$, 46469-74-3; $[Co(pn)_2CO_3]^+$, 29826-35-5; $[Co(12\text{-ane}N_4)(NO_2)_2]^+$, 89707-71-1; $[Co(9\text{-ane}N_3)_2]^{3+}$, 89637-25-2; $[Co(CH_3NH_2)_5Cl]^{2+}$, 30051-70-8; $[Ni(NH_3)_6]^{2+}$, 15365-74-9; $[Ni(en)_3]^{2+}$, 15390-99-5; $[Ni(pn)_3]^{2+}$, 18347-71-2; $[Ni(dien)_2]^{2+}$, 19358-75-9; $[Ni(dptn)_2]^{2+}$, 46933-28-2; $[Ni(9\text{-ane}N_3)_2]^{2+}$, 59034-11-6; $[Ni(en)_2]^{2+}$, 15390-98-4; $[Ni(daco)_2]^{2+}$, 41685-78-3; $[Ni(penten)]^{2+}$, 31252-70-7; $[Ni(en)(H_2O)_4]^{2+}$, 15615-30-2; $[Ni(en)_2(H_2O)_2]^{2+}$, 15554-67-3; $[Ni(pn)(H_2O)_4]^{2+}$, 31082-54-9; $[Ni(pn)_2(H_2O)_2]^{2+}$, 46140-10-7; $[Ni(dien)(H_2O)_3]^{2+}$, 15662-52-9; $[Ni(dptn)(H_2O)_3]^{2+}$, 69622-25-9; $[Ni(trien)(H_2O)_2]^{2+}$, 15662-53-0; $[Ni(2,3,2\text{-tet})(H_2O)_2]^{2+}$, 36530-71-9; $[Ni(cyclam)(H_2O)_2]^{2+}$, 68317-92-0; $[Ni(13\text{-ane}N_4)(H_2O)_2]^{2+}$, 78088-44-5.

(44) Fabbrizzi, L.; Paoletti, P.; Lever, A. B. P. *Inorg. Chem.* **1976**, *15*, 1502–1506.

(45) Johnson, C. K. "ORTEP", Report ORNL-3794; Oak Ridge National Laboratory: Oak Ridge, TN, 1965.

Cofacial Assembly of Metallomacrocycles as an Approach to Controlling Lattice Architecture in Low-Dimensional Molecular Solids. Chemical, Structural, Oxidation-State, Transport, and Optical Properties of the Coordination Polymer [Fe(phthalocyaninato)(μ-pyrazine)]$_n$ and the Consequences of Halogen Doping

Bruce N. Diel,[1a] Tamotsu Inabe,[1a] Narendra K. Jaggi,[1d] Joseph W. Lyding,[1b] Otto Schneider,[1c] Michael Hanack,*[1c] Carl R. Kannewurf,*[1b] Tobin J. Marks,*[1a] and Lyle H. Schwartz*[1d]

Contribution from the Department of Chemistry, the Department of Electrical Engineering and Computer Science, the Department of Materials Science and Engineering, and the Materials Research Center, Northwestern University, Evanston, Illinois 60201, and the Institute of Organic Chemistry, Lehrstuhl für Organische Chemie II, University of Tübingen, D-7400 Tübingen 1, West Germany. *Received September 6, 1983*

Abstract: This contribution reports the first integrated chemical and physicochemical study of the consequences of iodine doping on the cofacially joined metallomacrocyclic coordination polymers [Fe(Pc)(μ-pyz)]$_n$ (Pc = phthalocyaninato, pyz = pyrazine). Polymers $\{[Fe(Pc)(\mu\text{-pyz})]I_y\}_n$, $y \lesssim 3$, were prepared via the reaction of either [Fe(Pc)(μ-pyz)]$_n$ or Fe(Pc)(pyz)$_2$ with iodine, and stoichiometry was established by elemental analysis and TGA/DTA (the latter measurements evidence stepwise loss of I_2, which is rather weakly bound, and then pyrazine). X-ray diffractometry indicates that the I_2-doped polymer is not highly crystalline, but that the undoped polymer is readily regenerated upon iodine removal. Resonance Raman spectroscopy indicates, by the reduced nature of the iodine species, that the polymer has been oxidized, while both ^{57}Fe Mössbauer (which supports the $\{[Fe(Pc)(\mu\text{-pyz})I_y\}_n$ structural formulation) and ESR spectroscopy argue that the oxidation is largely ligand centered. Reflectance spectroscopy indicates that any plasmalike edge in the infrared is extremely weak, in marked contrast to previously studied $\{[M(Pc)O]I_{1.1}\}_n$ polymers, M = Si, Ge. Four-probe charge-transport measurements on polycrystalline samples reveal large increases (up to 10^6) in electronic conductivity with increasing dopant level ($\sigma(\max) \approx 0.1\ \Omega^{-1}\ cm^{-1}$ at 300 K); the dependence of conductivity upon dopant level suggests the importance of percolation. The conductivity is thermally activated, with the apparent activation energies decreasing with increasing dopant level. A detailed analysis of the temperature dependence yields results in agreement with fluctuation-induced carrier tunneling through parabolic potential barriers separating the conducting regions.

The construction of multimolecular arrays in which conjugated metallomacrocycles are joined by covalent bridge in a cofacial manner (A) represents a powerful device for controlling lattice architecture and electronic delocalization in low-dimensional

0002-7863/84/1506-3207$01.50/0

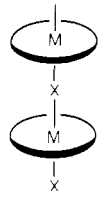

A

molecular solids. To date, the phthalocyanine macrocycle (Pc) has received the greatest attention, since under optimum conditions, such subunits are precursors for a class of "molecular metals".[2-4] Polymeric phthalocyanine systems which have been investigated include the following: group 4A polymers where M = Si, Ge, Sn, X = O,[4,5a,b] S,[5c] or a glycolate functionality;[3c,6] group 3A or 6B coordination polymers where M = Al, Ga, Cr, X = F;[7] and group 8 transition-metal coordination polymers where M = Fe, Co, Cr, Mn, Rh, X = CN[8] or a bridging bidentate organic ligand.[5b,9] In the former two classes of materials, doping by halogens or, in some cases, by other inorganic[4h,i,7e] or organic acceptors.[4c,h,i] is well understood and results in dramatic enhancements in electrical conductivity as well as in the appearance of the characteristic magnetic and optical signatures of a "molecular metal".

In contrast to the aforementioned state of knowledge, the dopant-related properties of the group 8 transition-metal phthalocyaninato coordination polymers have not yet been investigated, although this very large class of materials offers unique features in terms of alternative (and distinctly nonclassical[2-4]) conduction pathways,[9a,10,11] unusual stacking architecture (in particular, very large ring–ring interplanar spacings), and potentially informative built-in spectroscopic probes, e.g., Mössbauer-active nuclei. In this contribution, we present the first integrated chemical, spectroscopic, and charge-transport investigation of the prototypical member of the nitrogenous ligand-bridged transition-metal class of materials, $[Fe(Pc)(\mu\text{-pyz})]_n$. This study also represents the first Mössbauer spectroscopic examination of a low-dimensional metallomacrocyclic conductor. We focus here in particular on a number of properties of $[Fe(Pc)(\mu\text{-pyz})]_n$ as a function of incremental partial oxidation with iodine.

Table I. $\{[Fe(Pc)(pyz)]I_y\}_n$ Materials Prepared by Iodination of $[Fe(Pc)(pyz)]_n$

wt of $[Fe(Pc)(pyz)]_n$, mg	wt of I_2, mg	y[a] found
130	6.4	0.19
130	12.7	0.38
260	50.8	0.77
130	101.5	2.76[b]

[a] By microanalysis. [b] Significant loss of I_2 at room temperature; analysis after 1 week.

Table II. $\{[Fe(Pc)(pyz)]I_y\}_n$ Materials Prepared by Iodination of $Fe(Pc)(pyz)_2$

wt of $Fe(Pc)(pyz)_2$, mg	wt of I_2, mg	y[a] found
146	25.4	0.38
292	113.5	1.49
292	203	2.54

[a] By microanalysis.

Experimental Section

Elemental analyses were performed by Microtech Analytical Laboratories, Stokie, IL. The solvents benzene and chloroform were dried in an appropriate manner. The complex $Fe(Pc)(pyz)_2$ (pyz = pyrazine) and the polymer $[Fe(Pc)(pyz)]_n$ were prepared as described elsewhere.[9b-d]

Iodine Doping, Starting with $[Fe(Pc)(pyz)]_n$. A weighed quantity of the polymer $[Fe(Pc)(pyz)]_n$ and an appropriate amount of iodine were wet with a small amount of benzene (ca. 0.1 mL), and the resulting paste was vigorously ground with a mortar and pestle until the benzene evaporated. This procedure was then repeated twice more (total grinding time ~10–15 min) to yield a finely divided, black solid. Analytical data for these materials are compiled in Table I. Although the iodine in these compounds is weakly bound (it can be washed away with benzene), the physical properties are distinctly different from those of the starting material (see Results and Discussion) and are essentially the same as those for materials prepared by more conventional doping methodology.

Iodine Doping, Starting with $Fe(Pc)(pyz)_2$. To 10 mL of $CHCl_3$ containing a measured amount of iodine (see Table II) was added 146 mg (0.2 mmol) of $Fe(Pc)(pyz)_2$, which is slightly soluble in $CHCl_3$. After being stirred at room temperature for 24 h, the mixture was centrifuged and the supernatant (still containing some iodine) removed from the black precipitate. Analytical data for the $\{[Fe(Pc)(pyz)]I_y\}_n$ materials prepared in this manner are given in Table II.

X-ray Diffraction. X-ray powder diffraction patterns of all compounds studied were recorded on a Rigaku Geigerflex recording powder diffractometer using graphite monochromated, Ni-filtered Co or Cr $K\alpha$ radiation. The powders were pressed (8–10 tons on a ring press) into cylindrical pellets 13 mm in diameter and 1–2 mm thick. All patterns were recorded at a scanning rate of 0.25°/min. The apparatus was regularly calibrated by carefully recording the diffraction pattern of Si powder. The receiving slit was set at 0.6 mm and divergence and scattering slits set at 0.5° for $5° < 2\theta < 20°$, at 1° for $20° < 2\theta < 40°$, at 2° for $40° < 2\theta < 80°$, and at 4° for $80° < 2\theta$ in order to expose the maximum sample area.

(1) (a) Department of Chemistry and the Materials Research Center; (b) Department of Electrical Engineering and Computer Science and the Materials Research Center; (c) University of Tübingen; (d) Department of Materials Science and Engineering and the Materials Research Center.

(2) (a) Miller, J. S., Ed. "Extended Linear Chain Compounds"; Plenum Press: New York, 1982; Vol. 1–3. (b) Seymour, R. B., Ed. "Conductive Polymers", Polymer Science and Technology Series; Plenum Press: New York, 1981; Vol. 15. (c) Alcácer, L., Ed. "The Physics and Chemistry of Low-Dimensional Solids"; D. Reidel: Dordrecht, 1980. (d) Devreese, J. T.; Evrard, V. E.; Van Doren, V. E., Eds. "Highly Conducting One-Dimensional Solids"; Plenum Press: New York, 1979. (e) Hatfield, W. E., Ed. "Molecular Metals"; Plenum Press: New York, 1979. (f) Torrance, J. B. *Acc. Chem. Res.* **1979**, *12*, 79–86. (g) Miller, J. S.; Epstein, A. J. *Ann. N.Y. Acad. Sci.* **1978**, *313*.

(3) (a) Schramm, C. S.; Scaringe, R. P.; Stojakovic, D. R.; Hoffman, B. M.; Ibers, J. A.; Marks, T. J. *J. Am. Chem. Soc.* **1980**, *102*, 6702–6713. (b) Marks, T. J.; Kalina, D. W. In ref 2a, Vol. 1, pp 197–331. (c) Stojakovic, D. R. Ph.D. Thesis, Northwestern University, 1978.

(4) (a) Dirk, C. W.; Inabe, T.; Schoch, K. F., Jr.; Marks, T. J. *J. Am. Chem. Soc.* **1983**, *105*, 1539–1550. (b) Diel, B. N.; Inabe, T.; Lyding, J. W.; Schoch, K. F., Jr.; Kannewurf, C. R.; Marks, T. J. *Ibid.* **1983**, *105*, 1551–1567. (c) Dirk, C. W.; Schoch, K. F., Jr.; Marks, T. J.; Lyding, J. W. In "Molecular Electronic Devices"; Carter, F. L., Ed.; Plenum Press: New York, 1982; pp 195–210. (d) Diel, B. N.; Inabe, T., Lyding, J. W.; Schoch, K. F., Jr.; Kannewurf, C. R.; Marks, T. J. *Polym. Prepr. (Am. Chem. Soc., Div. Polym. Chem.)* **1982**, *23*, 124–125. (e) Dirk, C. W.; Mintz, E. A.; Schoch, K. F., Jr.; Marks, T. J. *J. Macromol. Sci., Chem.* **1981**, *A16*, 275–298. (f) Marks, T. J.; Schoch, K. F., Jr.; Kundalkar, B. *Synth. Met.* **1980**, 337–347. (g) Schoch, K. F., Jr.; Kundalkar, B. R.; Marks, T. J. *J. Am. Chem. Soc.* **1979**, *101*, 7071–7073. (h) Inabe, T.; Lyding, J. W.; Moguel, M. K.; Kannewurf, C. R.; Marks, T. J. *Mol. Cryst. Liq. Cryst.* **1983**, *93*, 355–367. (i) Inabe, T.; Lyding, J. W.; Moguel, M. K.; Marks, T. J. *J. Phys.* **1983**, *C3*, 625–631. (j) Burton, R. L.; Inabe, T.; Lyding, J. W.; Kannewurf, C. R.; Marks, T. J., submitted for publication.

(5) (a) Metz, J.; Pawlowski, G.; Hanack, M. *Z. Naturforsch., B* **1983**, *38B*, 378–382. (b) Schneider, O.; Metz, J.; Hanack, M. *Mol. Cryst. Liq. Cryst.* **1982**, *81*, 273–284. (c) Hanack, M.; Fischer, K. *Chem. Ber.* **1983**, *116*, 1860–1865.

(6) Dirk, C. W.; Marks, T. J., manuscript in preparation.

(7) (a) Kuznesof, P. M.; Wynne, K. J.; Nohr, R. S.; Kenney, M. E. *J. Chem. Soc., Chem. Commun.* **1980**, 121. (b) Nohr, R. S.; Kuznesof, P. M.; Wynne, K. J.; Kenney, M. E.; Siebenman, P. G. *J. Am. Chem. Soc.* **1981**, *103*, 4371–4377. (c) Nohr, R. S.; Wynne, K. J. *J. Chem. Soc., Chem. Commun.* **1981**, 1210. (d) Wynne, K. J.; Nohr, R. S. *Mol. Cryst. Liq. Cryst.* **1982**, *81*, 243–54. (e) Brant, P.; Nohr, R. S.; Wynne, K. J.; Weber, D. C. *Ibid.* **1982**, *81*, 255–263.

(8) (a) Metz, J.; Hanack, M. *J. Am. Chem. Soc.* **1983**, *105*, 828–830. (b) Schneider, O.; Hanack, M. *Z. Naturforsch. B*, in press.

(9) (a) Hanack, M.; Seelig, F. F.; Strähle, J. *Z. Naturforsch., A* **1979**, *34A*, 983–985. (b) Schneider, O.; Hanack, M. *Angew. Chem., Int. Ed. Engl.* **1980**, *19*, 392. (c) Schneider, O.; Hanack, M. *Ibid.* **1982**, *21*, 79. (d) Schneider, O.; Hanack, M. *Chem. Ber.* **1983**, *116*, 2088–2108. (e) Metz, J.; Schneider, O.; Hanack, M. *Spectrochim. Acta, Part A* **1982**, *38A*, 1265–1273. (f) Hanack, M.; Kobel, W.; Koch, J.; Metz, J.; Schneider, O. *Mol. Cryst. Liq. Cryst.* **1983**, *96*, 263–270. (g) Schneider, O.; Hanack, M. *Angew. Chem., Int. Ed. Engl.* **1983**, *22*, 784. (h) Hanack, M. *Chimia* **1983**, *37*, 238–245.

(10) (a) Seelig, F. F. *Z. Naturforsch., A* **1979**, *34A*, 986–982. (b) Seelig, F. F. *Mol. Cryst. Liq. Cryst.* **1982**, *81*, 285–291.

(11) Hanack, M.; Koch, J. *Chem. Ber.* **1983**, *116*, 2109–2114.

Raman Spectroscopy. Raman spectra of the iodine-doped polymers were recorded with Ar^+ excitation (5145 Å) using a Spex 1401 monochromator and photon counting detection. Calibration was with the laser exciting line or plasma emissions. The samples were studied as powders in 5-mm Pyrex tubes spinning at 1200 rpm using a 180° backscattering geometry. There was no evidence of decomposition after multiple scans on individual samples.

Transmission Infrared Spectroscopy. Transmission infrared spectra of halogen-doped polymers were recorded on Nujol mulls between KBr plates using Perkin-Elmer Model 283 or 599-B spectrometers and were calibrated with polystyrene film. Multiple scans were performed to check for possible decomposition.

Charge-Transport Measurements. Four-probe direct-current electrical conductivity measurements were routinely obtained for pressed pellet powder compactions of the undoped and doped polymers over the range $77 < T < 320$ K and for one sample over the range $4.2 < T < 320$ K. A computer-controlled system was employed to provide automated temperature control and data acquisition, and programmed as well as operator real-time decision-making capabilities. For this investigation, a sample holder was designed to accommodate the particular specimen geometry (1 mm × 1 mm × 5 mm pellets or 13 mm × 1 mm disks) and to facilitate making ohmic contacts. The material to be measured was ground with a mortar and pestle and then transferred to the pellet die and pressed under 8–10 tons pressure in a ring press (identical conditions with those employed for diffraction and reflectivity specimens). Sample pellets were mounted on a glass coverslip which was affixed to a copper heat sink by vacuum grease. Electrical connections were accomplished with 5-mil tungsten wires spring-loaded across the pellet surface and further joined with Aquadag. Contact separations were measured with a calibrated binocular microscope. Routinely, 3–4 specimens were processed for a given sample stoichiometry. Before a variable-temperature study was initiated, samples were tested at room temperature for ohmic behavior, low contact resistance, and any time-dependent behavior (which could indicate ion conduction). For 77 K measurement sequences, the temperature control was programmed to cycle from room temperature to 77 K (typically in 2 K steps) and then to return to above room temperature (320 K). Stable temperature control (±0.01 K) was established at each set point before data acquisition was initiated. For liquid helium measurements, samples were precooled to 4.2 K and then slowly brought to 100 K in steps ranging from 0.2 to 2.0 K. Routinely, 3–4 separate variable-temperature measurement runs were carried out for each sample to assess reproducibility and reversibility. At a given temperature, reproducibility was within 5%.

To check for possible ion conduction, an experiment was conducted with platinum blocking electrodes in which a dc current of 100 μA was passed through a 9.6-mg pellet of $\{[Fe(Pc)(pyz)]I_{2.10}\}_n$ for 80 h. Electrochemically, this represents 75 times the number of coulombs required to oxidize all of the I_5^- present to I_2. During this period, the conductivity of the pellet decreased by less than 1.2%.

Reflectance Spectroscopy. Reflectance spectra in the frequency range 300–4000 cm^{-1} were recorded with a Perkin-Elmer Model 180 infrared spectrophotometer. The instrument was operated in the double-beam mode and adjusted to yield a resolution of approximately 1.0 cm^{-1} at 4000 cm^{-1}. Calibration of this instrument was accomplished by means of a front surface aluminum mirror. All measurements were made at room temperature by using unpolarized radiation and at near-normal incidence.

Samples, which were prepared as described for the electrical transport measurements, were pressed (using polished dies) polycrystalline pellets in the shape of flat disks, 13 mm in diameter with thicknesses of 0.75–1.0 mm. In all arrangements, the area of the incident light beam was much less than the area of the sample; the reflective quality of the front surface showed no significant variation across the central surface area.

ESR Spectroscopy. Electron spin resonance experiments were carried out on a highly modified Varian E-4 X-band ESR spectrometer using 100-kHz field modulation. The field was calibrated with 2,2-diphenyl-1-picrylhydrazyl (DPPH, $g = 2.0036$). The cavity resonance frequency was measured to an accuracy of 5 ppm by a transfer oscillator technique.

TGA/DTA Measurements. Thermogravimetric and differential thermal analysis studies on the doped and undoped polymers were carried out with a Netzsch-Simultan thermoanalyzer, Model STA 429. Measurements were conducted under a nitrogen atmosphere with a heating rate of 2°/min. For DTA studies, Al_2O_3 was employed as the standard.

Mössbauer Spectroscopy. Mössbauer spectra were recorded at room temperature or 4.2 K in the constant acceleration mode by using an Austin Science Associates S-600 spectrometer in conjunction with a 512 channel ND-220 multichannel analyzer. All specimens had approximately the same effective thickness (0.10–0.13 mg/cm^2 of ^{57}Fe). Usually 6–8 × 10^5 counts per channel were accumulated with ca. 5% dips. Spectra were computer fitted by using a standard iterative, nonlinear least-squares algorithm. The results of fitting the spectra to a single quadrupolar doublet without any constraints are shown in Table V.

The estimated thickness broadening for all spectra, assuming a recoilless fraction of 0.5, varies from 0.015 to 0.020 mm/s, corresponding to a range of 0.10–0.13 mg/cm^2 of ^{57}Fe. Thus, a maximum line-width difference of 0.005 mm/s may be attributed to difference in sample thickness.

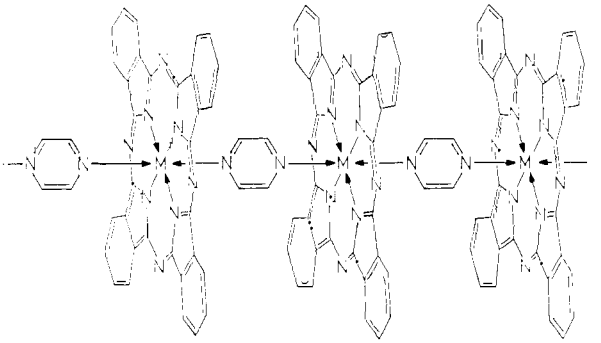

Figure 1. Schematic illustration of the structure of $[Fe(Pc)(\mu\text{-pyz})]_n$.

Table III. Powder X-ray Diffraction Data for μ-Pyrazine Polymers[a]

$\{[Fe(Pc)(pyz)]\cdot 0.5C_6H_6\}_n$[b]	$\{[Fe(Pc)(pyz)]\cdot 0.5C_6H_6\}_n$[c]	$\{[Fe(Pc)(pyz)]\cdot 0.3C_6H_5Cl\}_n$[d]
13.59 m	13.68 m	18.50 w
7.45 vw	7.42 vw	15.92 vw
6.27 m	6.28 m	13.55 s
5.80 m	5.85 m	12.34 vs
	5.64 w	10.12 vw
	5.07 w	6.76 w
4.14 vw	4.09 vw	6.14 m
3.42 w	3.42 s	5.45 w
3.14 vw		4.51 w
		4.11 w
		3.75 w
		3.41 m
		3.20 vw
		3.09 w

[a] *d* spacings in Å; s = strong, m = medium, w = weak, v = very. [b] Prepared by the method of eq 2, followed by washing with benzene. [c] Prepared by doping via the procedure of eq 5, followed by benzene washing. [d] Prepared by the method of eq 3.

Results

Polymer Synthesis and Structure. The polymer $[Fe(Pc)(\mu\text{-pyz})]_n$ (**1**) can be prepared as a dark violet solid from ferrous phthalocyanine and pyrazine via the methodology of eq 1 and 2 or of eq 3. The materials prepared by these two procedures have

$$Fe(Pc) \xrightarrow[\Delta]{\text{pyz (neat)}} Fe(Pc)(pyz)_2 \quad (1)$$

$$n Fe(Pc)(pyz)_2 \xrightarrow[\text{room temp}]{CHCl_3} [Fe(Pc)(pyz)]_n + n(pyz) \quad (2)$$

$$n Fe(Pc) + n(pyz) \xrightarrow[\Delta]{C_6H_5Cl \text{ or benzene}} [Fe(Pc)(pyz)]_n \quad (3)$$

been characterized by elemental analysis, TGA/DTA, infrared and far-infrared spectroscopy, UV-visible spectroscopy, and magnetic susceptibility measurements.[5b,9b-e] The compositions from the two synthetic procedures differ only in small amounts of included solvent (i.e., $\{[Fe(Pc)(pyz)]\cdot 0.5C_6H_6\}_n$, $\{[Fe(Pc)(pyz)]\cdot 0.3C_6H_5Cl\}_n$, with all data being consistent with the polymer architectural model shown in Figure 1.[5b,9] Quantitative infrared spectroscopic measurements of the degree of polymerization reveal that $n > 20$.[9e] In terms of crystal structure, powder diffraction data (Table III) now show that these polymers are highly crystalline and that the identity of the included solvent as well as reaction conditions give rise to detectable structural differences. Attempts at computer-assisted indexing of the diffraction data[4a,b] revealed that the $[Fe(Pc)(pyz)]_n$ polymers are *not* isostructural with the aforementioned $[M(Pc)O]_n$ or $[M(Pc)F]_n$ polymers. It

Table IV. Representative TGA/DTA Data for $\{[Fe(Pc)(pyz)]I_y\}_n$ Samples

	$y = 0.38$[a]	$y = 1.49$[a]	$y = 2.54$[a]
stage 1			
temp, °C	110–175	115–205	120–200
mass loss, %	5.6[b] (6.9)[c]	19.4[b] (22.5)[c]	29.6 (33.2)[c]
stage 2			
temp, °C	230–285	230–280	235–280
mass loss, %	11.3[d] (11.5)[e]	9.2[d] (9.5)[e]	7.9[d] (8.2)[e]
stage 3			
temp, °C		320–370	320–350
mass loss, %		2.6[f]	3.2[f]
total mass loss found, %	16.9	31.2	40.7
total mass loss calcd, %	18.4	32.0	41.4
residue	β-Fe(Pc)[g]	β-Fe(Pc)[g]	β-Fe(Pc)[g]

[a] By microanalysis. [b] Endotherm. [c] Quantity in parentheses is calculated weight decrease for iodine loss. [d] Endotherm. [e] Quantity in parentheses is calculated weight decrease for pyrazine loss. [f] No DTA signal observed. [g] Identified by infrared spectroscopy.

will be seen that other spectroscopic data are also in accord with the basic model in Figure 1.

Iodine Doping Process. Iodine-doped compounds of stoichiometry $\{[Fe(Pc)(pyz)]I_y\}_n$ can be synthesized either by treating the suspended, undoped polymer with iodine in benzene (eq 4) or by precipitating the polymer (cf. eq 2) from a $Fe(Pc)(pyz)_2$ solution containing iodine (eq 5). The stoichiometries of compounds prepared by these two procedures are given in Tables I and II, respectively. It will be seen that properties are rather insensitive to the method of preparation. The compositions of the doped μ-pyrazine polymers were established both by microanalysis (which also indicates the absence of appreciable included solvent) and TGA/DTA. The latter data, examples of which are given in Table IV, reveal three well-defined stages of weight loss. The first two correspond well to initial iodine loss, followed by pyrazine loss. The third weight loss is generally rather small. The infrared spectra of the thermal residues are in all cases identical with an authentic sample of β-Fe(Pc). The thermal stability of these compounds is somewhat higher than that of the $\{[M(Pc)F]I_y\}_n$ polymers (M = Al, Ga, Cr) and is comparable to that of the $\{[Si(Pc)O]I_y\}_n$ polymers.[7d] Chemical evidence, however, reveals that the iodine dopant is rather weakly bound in the $\{[Fe(Pc)(pyz)]I_y\}_n$ materials. Thus, the iodine can be removed by repeated washing with benzene to regenerate $\{[Fe(Pc)(pyz)]\cdot 0.5C_6H_6\}_n$ (identified by elemental analysis, infrared spectrum, and X-ray powder pattern). Such properties are reminiscent of the partially oxidized organic conductor (perylene)I_3.[12]

$$[Fe(Pc)(pyz)]_n + (ny/2)I_2 \xrightarrow{\text{benzene}} \{[Fe(Pc)(pyz)]I_y\}_n \quad (4)$$

$$nFe(Pc)(pyz)_2 + (ny/2)I_2 \xrightarrow{CHCl_3} \{[Fe(Pc)(pyz)]I_y\}_n + n(pyz) \quad (5)$$

The nature of the iodine doping process was also investigated by X-ray powder diffractometry. Using either of the aforementioned doping methodologies, it was found that incremental iodination resulted in the progressive diminution of the pattern of the undoped phase. The doped polymers are not highly crystalline (as in the case of the $\{[M(Pc)O]I_y\}_n$ materials[4]), and by $y \approx 2$, only a broad, diffuse diffraction pattern is observed. As noted above, however, repeated washing with benzene removes the iodine and regenerates the diffraction pattern of $\{[Fe(Pc)(pyz)]\cdot 0.5C_6H_6\}_n$.

Doped Polymers. Resonance Raman Spectroscopy. Resonance Raman spectra of the $\{[Fe(Pc)(pyz)]I_y\}_n$ materials, studied as a function of y, reveal strong scattering at 173 and 107 cm^{-1}, which is essentially invariant with y (up to $y \approx 3.0$). A typical spectrum

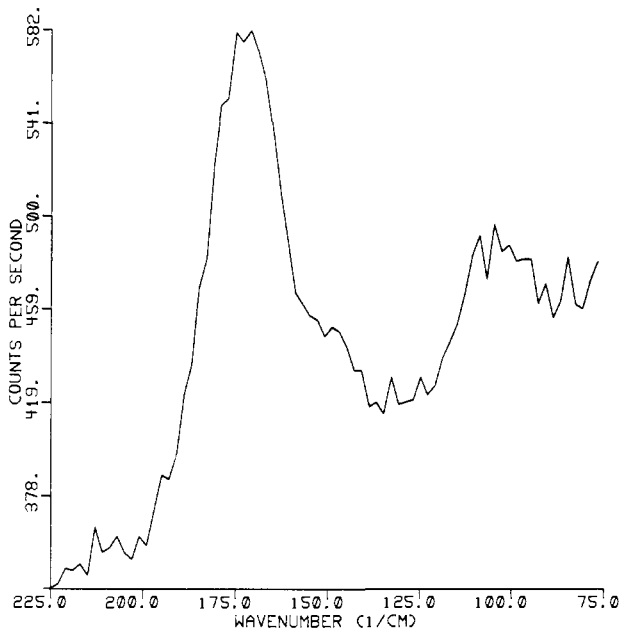

Figure 2. Resonance Raman spectrum of $\{[Fe(Pc)(\mu\text{-pyz})]I_{2.54}\}_n$ in the polyiodide stretching region with 5145-Å excitation.

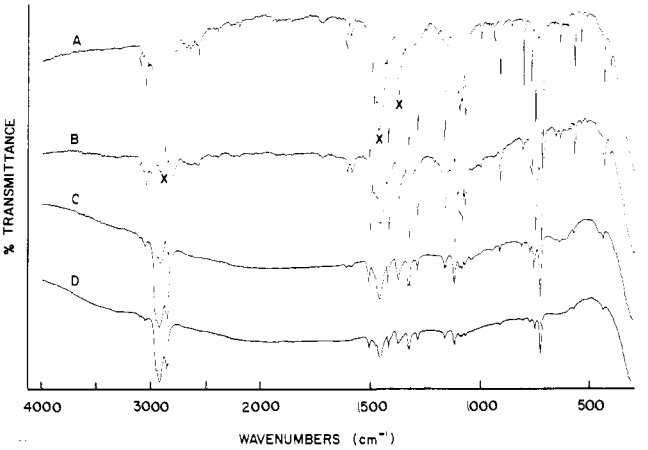

Figure 3. Transmission infrared spectra of $\{[Fe(Pc)(\mu\text{-pyz})]I_y\}$ as a function of incremental iodine doping. (A) $y = 0.00$; (B) $y = 0.38$; (C) $y = 1.49$; (D) $y = 2.54$. Bands labeled X are due to Nujol.

($y = 2.54$) is shown in Figure 2. This type of scattering pattern has been observed before (e.g., (perylene)I_3) and has been associated on the basis of structurally well-characterized model compounds as well as iodine-129 Mössbauer spectroscopy with polyiodides having I_2 units coordinated to I_3^- (e.g., B or C).[3b,12,13]

$$\underset{B}{I\text{–}I\cdots I\text{–}\bar{I}\text{–}I} \qquad \underset{C}{I\text{–}I\cdots I\text{-}\cdot\bar{I}\text{–}I}$$

Neither the number of coordinated I_2 moieties nor the degree to which the triodide units are distorted can be quantitatively derived from the Raman data alone. Clearly, however, the iodine doping has resulted in partial oxidation of the $[Fe(Pc)(pyz)]_n$ array, although the degree of oxidation per y is not as great as in the $\{[M(Pc)O]I_y\}_n$ series where iodine is present as I_3^- for $y < 1.1$.

Doped Polymers. Transmission Infrared and Specular Reflectance Spectroscopy. Transmission infrared spectra of $[Fe(Pc)(pyz)]_n$ are shown in Figure 3 as a function of iodine doping level. In the case of the $[M(Pc)O]_n$ polymers where M = Si and Ge, incremental iodine doping is accompanied by the progressive growth of a broad electronic absorption in the infrared.[4b,7] Such behavior is observed in a number of other conductive polymer

(12) Teitelbaum, R. C.; Ruby, S. L.; Marks, T. J. *J. Am. Chem. Soc.* **1979**, *101*, 7569–7573 and references therein.

(13) Teitelbaum, R. C.; Ruby, S. L.; Marks, T. J. *J. Am. Chem. Soc.* **1980**, *102*, 3322–3328.

Table V. Mössbauer Data for Fe(Pc)(pyz) Compounds

material	temp, K	δ,[a,b] mm/s	QS,[b] mm/s	W1,[b,c] mm/s	W2,[b,c] mm/s
$Fe(Pc)(pyz)_2$	298	0.500 (2)	2.006 (2)	0.252 (4)	0.248 (4)
$\{[Fe(Pc)(pyz)]\cdot 0.3C_6H_5Cl\}_n$	298	0.500 (2)	2.054 (2)	0.282 (4)	0.308 (4)
$\{[Fe(Pc)(pyz)]I_{0.38}\}_n$[d]	298	0.500 (2)	2.048 (2)	0.276 (4)	0.290 (4)
$\{[Fe(Pc)(pyz)]I_{0.77}\}_n$[d]	298	0.500 (2)	2.042 (2)	0.284 (4)	0.296 (4)
$\{[Fe(Pc)(pyz)]I_{0.77}\}_n$[d]	4.2	0.580 (2)	1.900 (2)	0.390 (4)	0.390 (4)
$\{[Fe(Pc)(pyz)]I_{2.76}\}_n$[d]	298	0.498 (2)	2.034 (2)	0.302 (4)	0.318 (4)
$\{[Fe(Pc)(pyz)]\cdot 0.5C_6H_6\}_n$	298	0.500 (2)	2.009 (2)	0.278 (4)	0.300 (4)
$\{[Fe(Pc)(pyz)]I_{1.49}\}_n$[e]	298	0.492 (2)	2.000 (2)	0.299 (4)	0.322 (4)
$\{[Fe(Pc)(pyz)]I_{2.54}\}_n$[e]	298	0.491 (2)	1.990 (2)	0.284 (4)	0.300 (4)

[a] Relative to sodium nitroprusside. [b] Fit to a single quadrupolar doublet. [c] Line width. [d] Prepared by the procedure of eq 4. [e] Prepared by the procedure of eq 5.

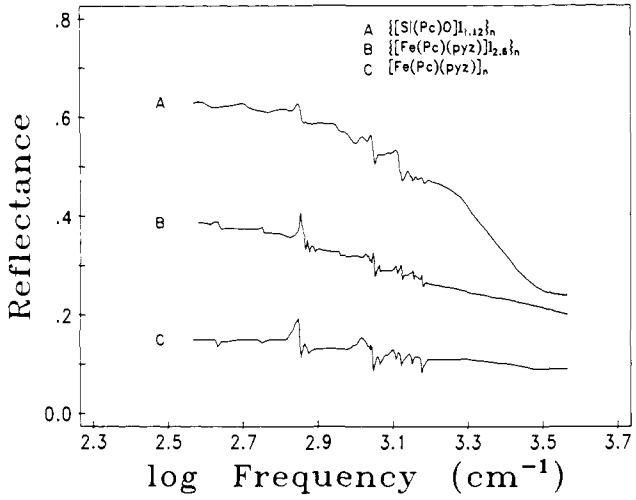

Figure 4. Optical reflectance spectra of polycrystalline samples: (A) $\{[Si(Pc)O]I_{1.12}\}_n$ from ref 4b; (B) $\{[Fe(Pc)(pyz)]I_{2.60}\}_n$; (C) $[Fe(Pc)(pyz)]_n$. Successive plots are displayed vertically by +0.10 reflectance unit.

systems as well.[14] Relative to the 750-cm^{-1} phthalocyanine skeletal mode, the transition maximum at approximately 2000 cm^{-1} is ca. 3 times more intense for M = Si than for M = Ge. In the present case, it can be seen that any electronic absorption is significantly weaker than in the group 4A polymers. Relative to the 750-cm^{-1} mode in $\{[Ge(Pc)O]I_{1.1}\}_n$, the absorption is ca. one-fifth to one-tenth as intense.

The group 4A polymers also exhibit a plasmalike edge in the reflectivity spectrum (ca. 3600 cm^{-1} for Si; ca. 3200 cm^{-1} for Ge) which progressively grows in intensity as the dopant level increases.[4b] These features could be analyzed within the context of a simple Drude free electron model to extract approximate tight-binding bandwidth information.[4b] Optical reflectance spectra for pressed pellet, polycrystalline samples of $[Fe(Pc)(pyz)]_n$, $\{[Fe(Pc)(pyz)]I_{2.60}\}_n$, and $\{[Si(Pc)O]I_{1.12}\}_n$ are shown in Figure 4. It can be seen that any plasmalike feature in the $\{[Fe(Pc)(pyz)]I_{2.60}\}_n$ spectrum is exceedingly weak and obscured by molecular features. For these reasons, no quantitative analysis of the reflectivity data was undertaken, and the reflectivity behavior suggests considerably less of a phthalocyanine π electron band structure in the present materials.

In accord with the other chemical and spectral observations, the relatively modest changes in the infrared spectral band positions and relative intensities upon doping suggest no great alterations in the $[Fe(Pc)(pyz)]_n$ architecture. Similar behavior was noted previously for $[Si(Pc)O]_n$ and $[Ge(Pc)O]_n$, although studies of $[Sn(Pc)O]_n$ revealed destruction of the Sn–O bonds upon iodine doping.[4b]

Mössbauer Spectroscopy. An extensive literature now exists on ^{57}Fe Mössbauer spectroscopy of iron phthalocyanine complexes.[15-17] For Fe(II),[15] hyperfine interaction parameters fall into three well-defined categories for complexes of the type Fe(Pc), $Fe(Pc)L_2$, and Fe(Pc)(CO)L. Within each category, the isomer shift (δ) is essentially independent of the identity of the axial ligand, i.e., δ = 0.50–0.54 mm/s for $Fe(Pc)L_2$ and 0.35–0.38 mm/s for Fe(Pc)(CO)L, where L is a nitrogen, oxygen, or sulfur donor. In contrast, quadrupole splittings (QS) fall over a much broader range for such complexes, i.e., 1.75–2.40 mm/s for $Fe(Pc)L_2$ and 1.02–1.82 mm/s for Fe(Pc)(CO)L. For $Fe(Pc)L_2$ complexes with L a nitrogenous ligand, QS = 1.84–2.19 mm/s.[15]

In Table V are set our Mössbauer data for the $Fe(Pc)(pyz)_2$, $[Fe(Pc)(pyz)]_n$, and $\{[Fe(Pc)(pyz)]I_y\}_n$ materials. All of the spectra are simple quadrupole-split doublets. Beginning with $Fe(Pc)(pyz)_2$ and $[Fe(Pc)(pyz)]_n$, it can be seen that the hyperfine parameters are very similar and within the range of published $Fe(Pc)L_2$ complexes. This result is in accord with nearly identical, low-spin octahedral Fe(II) environments and supports the polymer structural model of Figure 1. As regards polymer purity, the Mössbauer data for $[Fe(Pc)(pyz)]_n$ indicate that extraneous Fe(Pc) (α-Fe(Pc) δ = 0.46 (1) mm/s, QS = 2.49 (1) mm/s; β-Fe(Pc) δ = 0.48 (1) mm/s, QS = 2.68 (1) mm/s)[15c] is present in quantities less than 2% of the total iron. It can also be seen in Table V that the line widths of the polymer exceed those in $Fe(Pc)(pyz)_2$ by a significant increment. Although this may indicate the presence of multiple, slightly nonequivalent iron environments, the present data do not allow a rigorous analysis to be conducted.

Iodine doping of the polymer has only a small effect on the Mössbauer hyperfine parameters (Table V). Thus, while the isomer shift remains nearly constant upon incremental doping, the QS decreases almost monotonically from 2.054 to 2.031 mm/s. These results argue that the polymer structure of Figure 1 remains intact upon iodination. Furthermore, the oxidation involves orbitals that are *not* predominantly metal in character. This result parallels the $[M(Pc)O]_n$[4] and Ni(Pc)I[3a] systems where partial oxidation involves orbitals which are largely ligand in parentage. This electronic structure of course contrasts the low-dimensional materials such as $K_2Pt(CN)_4Br_{0.3}$ class,[18] where the mixed valence is exclusively metal-centered. The $\{[Fe(Pc)(pyz)]I_{0.77}\}_n$ Mössbauer spectrum at 4.2 K (Table V) is completely consistent with the

(14) (a) Nohr, R. S.; Kuznesof, P. M.; Wynne, K. J.; Kenney, M. E.; Siebenman, P. G. *J. Am. Chem. Soc.* **1981**, *103*, 4371–4377. (b) Bozio, R.; Pecile, C. In "The Physics and Chemistry of Low-Dimensional Solids"; Alcâcer, L., Ed.; D. Reidel: Dordrecht, 1980; pp 165–186. (c) Fincher, C. R., Jr.; Ozaki, M.; Heeger, A. J.; MacDiarmid, A. G. *Phys. Rev. B* **1979**, *19*, 4140–4148. (d) Wheland, R. C.; Gillson, J. L. *J. Am. Chem. Soc.* **1976**, *98*, 3916–3925. (e) Tanner, D. B.; Jacobsen, C. S.; Garito, A. F.; Heeger, A. J. *Phys. Rev. B* **1976**, *13*, 3381–3404.

(15) (a) Calderazzo, F.; Pampaloni, G.; Vitali, D.; Pelizzi, G.; Collamati, I.; Frediani, S.; Serra, A. M. *J. Organomet. Chem.* **1980**, *191*, 217–242 and references therein. (b) Calderazzo, F.; Frediani, S.; James, B. R.; Pampaloni, G.; Reimer, K. J.; Sams, J. R.; Serra, A. M.; Vitali, D. *Inorg. Chem.* **1982**, *21*, 2302–2306. (c) Srivastava, T. S.; Przybylinski, J. L.; Nath, A. *Ibid.* **1974**, *13*, 1562–1564.

(16) (a) Taube, R. *Pure Appl. Chem.* **1974**, *38*, 427–438. (b) Taube, R.; Drevs, H.; Fluck, E.; Kuhn, P.; Brauch, K. F. *Z. Anorg. Allg. Chem.* **1969**, *364*, 297–316. (c) Myers, J. F.; Canham, G. W. R.; Lever, A. B. P. *Inorg. Chem.* **1975**, *14*, 461–468.

(17) For results on analogous porphyrin complexes, see the following recent references: (a) Scheidt, W. R.; Geiger, D. K.; Hayes, R. G.; Lang, G. *J. Am. Chem. Soc.* **1983**, *105*, 2625–2632. (b) English, D. R.; Hendrickson, D. N.; Suslick, K. G. *Inorg. Chem.* **1983**, *22*, 367–368. (c) Phillippi, M. A.; Goff, H. M. *J. Am. Chem. Soc.* **1982**, *104*, 6026–6034.

(18) Williams, J. M. In ref 2a, Vol. 3.

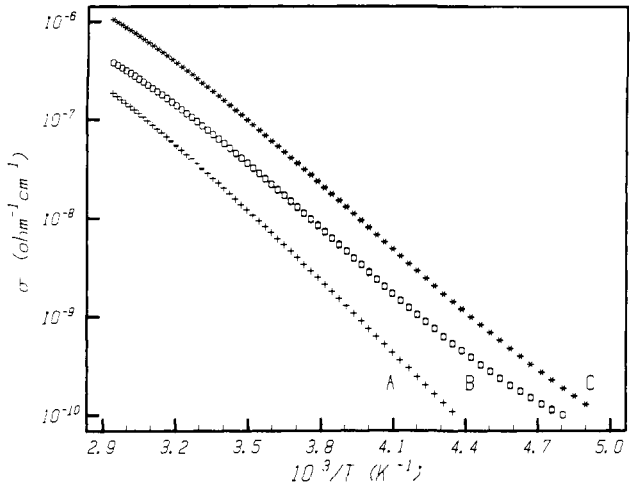

Figure 5. Temperature dependence of $[Fe(Pc)(\mu\text{-pyz})]_n$ electrical conductivity as a function of polymerization method. (A) Prepared by the procedure of eq 2. (B) Prepared by the procedure of eq 3 in C_6H_5Cl. (C) Prepared by the procedure of eq 3 in benzene.

above interpretation, with no evidence for grossly nonequivalent iron environments or trapped Fe(III) valence[16,17] (Robin–Day class II[19]) at this temperature. Thus, the small increase in isomer shift of 0.08 mm/s on going to 4.2 K is readily attributable to a second-order Doppler effect and is expected for $Fe(Pc)L_2$ complexes.[15] The slight decrease in QS by 0.14 mm/s is also typical behavior for $Fe(Pc)L_2$ complexes.[15] In regard to the "cleanliness" of $[Fe(Pc)(pyz)]_n$ partial oxidation, the present Mössbauer data place the presence of extraneous (i.e., giving separate signals) Fe(III)(Pc)[16] (e.g., Fe(Pc)Br: δ = 0.37 mm/s, QS = 3.16 mm/s)[16a] or other Fe(Pc) halogenation products[3c,16c,20] (e.g., $Fe(Pc)Cl_2$: δ = 0.35 mm/s, QS = 2.15 mm/s)[16c] below the ca. 2% level.

Electron Spin Resonance Spectroscopy. A considerable body of ESR data presently exists for macrocyclic iron (ferric) complexes in a wide variety of coordination environments.[21] Powder ESR spectra of $\{[Fe(Pc)(pyz)]I_{2.29}\}_n$ at either room temperature or 77 K conform to none of the above, previously observed Fe(III) patterns. At room temperature, superimposed broad (line width $\approx$ 400 G) and sharp (line width 50 G) signals, centered at g = 2.036, are observed. At 77 K, the line width of the broad component narrows to ca. 100 G, while the narrow component remains essentially unchanged. The signals are both centered at $g \approx 2.015$. These results are inconsistent with localized, static ferric porphyrin-like complexes having either conventional high- or low-spin structures[21] and are more suggestive of considerable π-radical-cation character for the partially oxidized state[22] (in accord with the above Mössbauer results). However, the uncertainties in the $\{[Fe(Pc)(pyz)]I_y\}_n$ structures, purities, and doping homogeneity necessarily render such conclusions, drawn from isotropic powder data, presently qualitative in nature. Further studies are in progress.

Doped Polymers. Charge Transport. Variable-temperature dc electrical conductivity measurements on the undoped and doped $\{[Fe(Pc)(pyz)]\}_n$ materials were performed in the four-probe geometry, using compressed polycrystalline samples (pellets similar or identical with those employed for the diffraction and reflectivity investigations). Although measurements on samples in this form are not as desirable for a low-dimensional material as those on well-formed single crystals (compaction measurements reflect averaging over all crystallographic orientations as well as inter-

Table VI. Pressed-Powder Electrical Conductivity Data for $\{[Fe(Pc)(pyz)]I_y\}_n$ Samples at Room Temperature

compd	σ_{RT}, Ω^{-1} cm^{-1}	activation energy, Δ,[a] eV
$[Fe(Pc)(pyz)]_n$[b]	7.79×10^{-8}	0.404
$\{[Fe(Pc)(pyz)]I_{0.19}\}_n$[c]	9.31×10^{-4}	0.139
$\{[Fe(Pc)(pyz)]I_{0.38}\}_n$[c]	2.58×10^{-3}	0.116
$\{[Fe(Pc)(pyz)]I_{0.77}\}_n$[c]	8.63×10^{-3}	0.079
$\{[Fe(Pc)(pyz)]I_{2.10}\}_n$[c]	7.55×10^{-3}	0.080
$\{[Fe(Pc)(pyz)]I_{2.76}\}_n$[c]	2.33×10^{-2}	0.065
$\{[Fe(Pc)(pyz)]I_{0.38}\}_n$[d]	4.60×10^{-4}	0.141
$\{[Fe(Pc)(pyz)]I_{1.49}\}_n$[d]	5.99×10^{-3}	0.053
$\{[Fe(Pc)(pyz)]I_{2.10}\}_n$[d]	1.28×10^{-1}	0.033
$\{[Fe(Pc)(pyz)]I_{2.54}\}_n$[d]	1.90×10^{-1}	0.045

[a] Calculated by least-squares fit to eq 6 for data from 96–300 K. [b] Sample B of Figure 5. [c] Prepared by the procedure of eq 4. [d] Prepared by the procedure of eq 5.

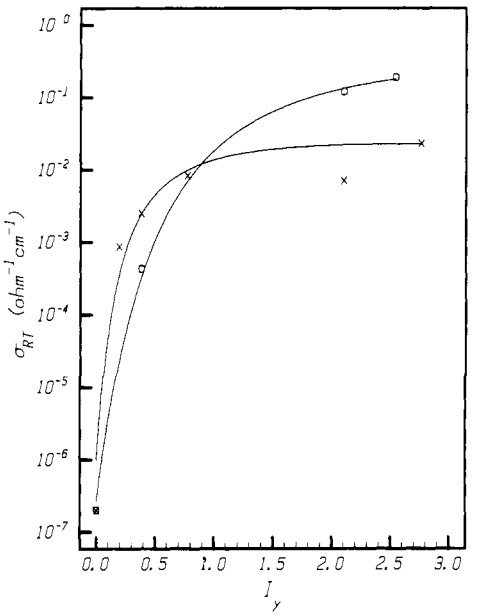

Figure 6. Electrical conductivity of polycrystalline $\{[Fe(Pc)(\mu\text{-pyz})]I_y\}_n$ samples as a function of iodine dopant level, y. X samples doped by the procedure of eq 4. O samples doped by the procedure of eq 5. The lines through the data points are drawn as a guide to the eye.

particle contact resistance), important information can nevertheless be obtained.[4] Furthermore, a large body of empirical observations now suggests that single-crystal conductivities of low-dimensional materials are almost invariably a factor of 10^2–10^3 greater along the stacking axis (the high-conductivity direction) than as measured for compressed polycrystalline samples. Thus meaningful comparisons can be drawn between different materials.[4b,23]

The charge-transport behavior of the $[Fe(Pc)(pyz)]_n$ polymers was first investigated to obtain information on the undoped materials. As can be seen in Figure 5, room-temperature conductivities are on the order of 10^{-6}–10^{-7} Ω^{-1} cm^{-1} and are not particularly sensitive to the mode of polymer synthesis (i.e., eq 1, 2, or 3). The room-temperature results differ only slightly from previously reported conductivities,[9c] which were measured under different conditions. The polymer conductivity is approximately 10^5–10^7 greater than that reported[9b] for $Fe(Pc)(pyz)_2$. The temperature dependence of the polymer conductivity can be fit to a model for thermal activation (eq 6) and derived activation

$$\sigma = Ae^{-(\Delta/kT)} \quad (6)$$

energies (Δ) are set out in Table VI. It can be seen that the activation energies are within experimental error invariant to the synthetic methodology.

Upon incremental doping with iodine, samples of $[Fe(Pc)(pyz)]_n$ prepared by either procedure exhibit rapid and roughly parallel increases in electrical (electronic) conductivity (Figure 6).

(19) (a) Day, P. In "Low-Dimensional Cooperative Phenomena"; Keller, H. J., Ed.; Plenum Press: New York, 1974; pp 191–214. (b) Robin, M. B.; Day, P. *Adv. Inorg. Chem. Radiochem.* **1967**, *10*, 247–422.

(20) Kim, J. R.; Stojakovic, D. R.; Hoffman, B. M.; Marks, T. J.; Schwartz, L. H., unpublished results.

(21) (a) Quinn, R.; Nappa, M.; Valentine, J. S. *J. Am. Chem. Soc.* **1982**, *104*, 2588–2595 and references therein. (b) Mashiko, T.; Reed, C. A.; Haller, K. J.; Kastner, M. E.; Scheidt, W. R. *Ibid.* **1981**, *103*, 5758–5767 and references therein. (c) Palmer, G. In "The Porphyrins"; Dolphin, D., Ed. Academic Press: New York, 1979; Vol. IV, Part B, pp 313–353.

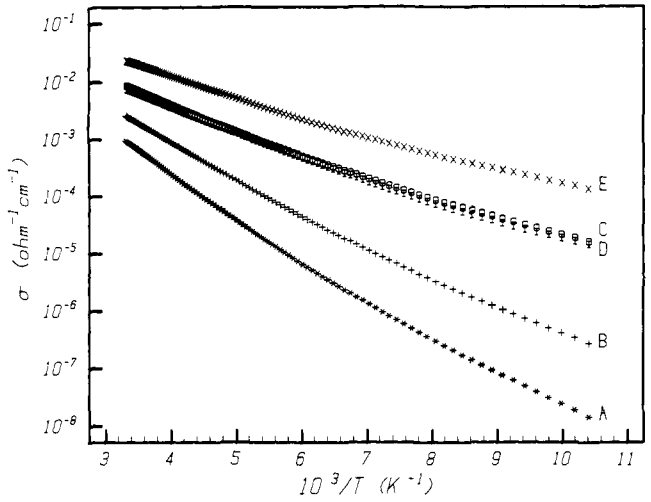

Figure 7. Electrical conductivity of polycrystalline $\{[Fe(Pc)(\mu\text{-pyz})]I_y\}_n$ samples prepared by the procedure of eq 4. (A) $y = 0.19$; (B) $y = 0.38$; (C) $y = 0.77$; (D) $y = 2.10$; (E) $y = 2.76$.

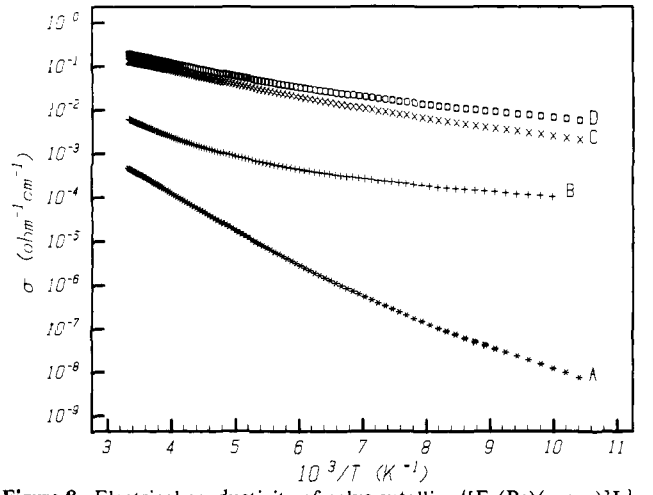

Figure 8. Electrical conductivity of polycrystalline $\{[Fe(Pc)(\mu\text{-pyz})]I_y\}_n$ samples prepared by the procedure of eq 5. (A) $y = 0.38$; (B) $y = 1.49$; (C) $y = 2.10$; (D) $y = 2.54$.

Limiting values of the $\{[Fe(Pc)(pyz)]I_y\}_n$ conductivity are reached by $y \approx 2$, with $\sigma \approx 10^{-1}$–10^{-2} Ω^{-1} cm^{-1}. For $\{[M(Pc)O]I_y\}_n$, limiting conductivity is reached at $y \approx 1.1$ with $\sigma \approx 1$ Ω^{-1} cm^{-1} (M = Si) and $\approx 10^{-1}$ Ω^{-1} cm^{-1} (M = Ge).[4b] For the group 4A polymers, the σ vs. y plots could be fit to a simple percolation model,[24] consistent with the inhomogeneous character of the doping process. Sufficient data were not available in the present case for such a numerical analysis. Qualitatively, however, it appears that the conductivity vs. dopant level relationship for the $\{[Fe(Pc)(pyz)]I_y\}_n$ polymer is rather similar to that of the $\{[M(Pc)O]I_y\}_n$ materials.

The temperature dependence of the conductivity for $\{[Fe(Pc)(pyz)]I_y\}_n$ samples doped by the two different procedures is shown in Figures 7 and 8. Several generalizations can be made. First, the transport characteristics for a given doping level are not significantly sensitive to the doping methodology. Second, the plots conform roughly at higher temperatures to a thermally activated model for charge transport. Fitting of the data by least-squares techniques to eq 6 yields the phenomenological

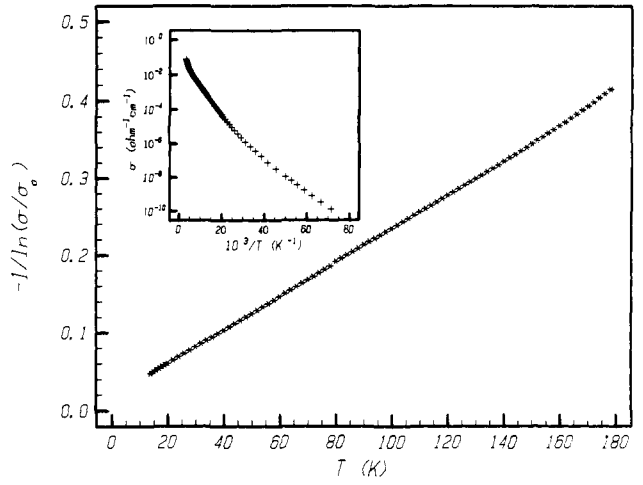

Figure 9. Variable-temperature conductivity data for $\{[Fe(Pc)(\mu\text{-pyz})]I_{2.60}\}_n$ plotted in accordance with the fluctuation-induced tunneling model of eq 7. Inset: the same data plotted in a standard log σ vs. $1/T$ format.

activation energies (Δ) compiled in Table VI. It can be seen that Δ falls with increasing dopant level. Similar behavior has been noted for the $\{[M(Pc)O]I_y\}_n$ materials[4b] and several other conductive polymer systems.[14a,23a,b,25]

Closer inspection of Figures 7 and 8 reveals that the plots are only approximately linear and that a "leveling off" of the log σ vs. $1/T$ relationship occurs at lower temperatures. This behavior is reminiscent of the $\{[M(Pc)O]I_y\}_n$ systems,[4b] polycrystalline Ni(Pc)I samples,[4b] and doped polyacetylene[26] and suggests finite conductivity at zero temperature. In the aforementioned systems, the data could be satisfactorily fit to a fluctuation-induced carrier tunneling model,[26,27] which describes the charge-transport behavior of conductive regions separated by small potential barriers. For the case of parabolic potential barriers,[26a] the conductivity should conform to eq 7, where T_1 represents an effective barrier activation

$$\sigma = \sigma_0 e^{-|T_1/(T+T_0)|} \tag{7}$$

energy and T_0 is a term describing the remnant elastic tunneling at zero temperature. Shown in Figure 9 are the results of plotting variable-temperature (14–180 K) conductivity data for $\{[Fe(Pc)(pyz)]I_{2.60}\}_n$ in a $-[\ln(\sigma/\sigma_0)]^{-1}$ vs. T format. The linearity at low temperatures is in accord with the fluctuation-induced tunneling model, while the higher temperature behavior is in a range where the model[26a] does not strictly apply. Fitting the data over several temperature intervals where it appeared visually to be approximately linear (14–110 K to 14–150 K) yielded the parameters $\sigma_0 = 0.155$ (4) Ω^{-1} cm^{-1}, $T_1 = 460$ (4)°, and $T_0 = 7.6$ (2)° where the standard deviations are derived from the fitting procedure. An analysis of the $\{[M(Pc)O]I_y\}_n$ data[4b] yielded similar parameters.

Conclusions

This study extends the halogen partial oxidation methodology to another large and important class of cofacially joined metallomacrocyclic polymers. Perhaps the most interesting observation is that, despite the rather large interplanar phthalocyanine–phthalocyanine spacings in a single $[Fe(Pc)(\mu\text{-pyz})]_n$ chain, the doping effects very large increases in electronic electrical conductivity. Maximum conductivities of polycrystalline samples are comparable to those of polycrystalline $\{[Ge(Pc)O]I_y\}_n$ specimens.

(22) Fajer, J.; Davis, M. S. In ref 21c, pp 197–256.
(23) (a) Chiang, C. K.; Druy, M. A.; Gau, S. C.; Heeger, A. J.; Louis, E. J.; MacDiarmid, A. G. *J. Am. Chem. Soc.* **1978**, *100*, 1013–1015. (b) Chiang, C. K.; Park, Y. W.; Heeger, A. J.; Shirakawa, H.; Louis, E. J.; MacDiarmid, A. G. *J. Chem. Phys.* **1978**, *69*, 5098–5104. (c) Farges, J. P.; Brau, A.; Gutmann, F. *J. Phys. Chem. Solids* **1972**, *33*, 1723–17256.
(24) (a) Wegner, G. *Angew. Chem., Int. Ed. Engl.* **1981**, *20*, 361–381. (b) Lagues, M.; Sauterey, C. *J. Phys. Chem.* **1980**, *84*, 3503–3508. (c) Seager, C. H.; Pike, G. E. *Phys. Rev. B* **1974**, *10*, 1435–1446 and references therein. (d) Kirkpatrick, S. *Rev. Mod. Phys.* **1973**, *45*, 574–588 and references therein.
(25) (a) Chance, R. R.; Shacklette, L. W.; Miller, G. G.; Ivory, D. M.; Sowa, J. M.; Elsenbaumer, R. L.; Baughman, R. H. *J. Chem. Soc., Chem. Commun.* **1980**, 348–349. (b) Audenaert, M. Gusman, C.; Deltour, R. *Phys. Rev. B* **1981**, *24*, 7380–7382 and references therein.
(26) (a) Sheng, P. *Phys. Rev. B* **1980**, *21*, 2180–2195. (b) Park, Y.-W.; Heeger, A. J.; Druy, M. A.; MacDiarmid, A. G. *J. Chem. Phys.* **1980**, *73*, 946–957 and references therein.
(27) (a) Mott, N. F. "Metal-Insulator Transitions"; Taylor and Francis: London, 1974; pp 30–42. (b) Movaghar, B.; Shirmacher, W. *J. Phys. C* **1981**, *14*, 859–880.

All evidence points to an iodine oxidation process which is largely ligand centered (indeed, Mössbauer spectral parameters are virtually insensitive to doping) and which does not produce the type of π electron band structure found in the partially oxidized group 4 $\{[M(Pc)O]I_y\}_n$ polymers. These results suggest very interesting and substantial differences in structure and charge-transport mechanism vis-ã-vis other low-dimensional, partially oxidized metallomacrocycles. Further efforts to characterize these differences are in progress.

Acknowledgment. We thank the NSF (Grant DMR79-23573 through the Materials Research Center of Northwestern University), the Deutsche Akademische Austauschdienst, and Stiftung Volkswagenwerk (West Germany) for support of this research.

Registry No. $Fe(Pc)(pyz)_2$, 74558-67-1; $[Fe(Pc)(\mu\text{-pyz})]_n$, 74591-77-8; iodine, 7553-56-2.

η^2-Acyl Coordination and β-C-H Interaction in Acyl Complexes of Molybdenum. Crystal and Molecular Structures of $Mo(\eta^2\text{-}COCH_2SiMe_3)Cl(CO)(PMe_3)_3$ and $Mo(COCH_3)(S_2CNMe_2)(CO)(PMe_3)_2$

Ernesto Carmona,*† Luis Sánchez,† José M. Marín,† Manuel L. Poveda,† Jerry L. Atwood,*‡ Ralph D. Priester,‡ and Robin D. Rogers*§

Contribution from the Departamento de Química Inorgánica, Facultad de Química, Universidad de Sevilla, Sevilla, Spain, the Department of Chemistry, University of Alabama, University, Alabama 35486, and the Department of Chemistry, Northern Illinois University, DeKalb, Illinois 60115. *Received October 31, 1983*

Abstract: A number of acyl complexes of composition $Mo(\eta^2\text{-}COR)X(CO)(PMe_3)_3$ (X = Cl, Br, I or NCO; R = CH_3, CH_2SiMe_3, CH_2CMe_3, CH_2CMe_2Ph) have been prepared by reaction of $MoCl_2(CO)_2(PMe_3)_3$ with the corresponding Grignard or lithium reagents. IR and NMR studies suggest dihapto coordination of the acyl group to the molybdenum center, and this has been confirmed by X-ray crystallography for $MoCl(\eta^2\text{-}COCH_2SiMe_3)(CO)(PMe_3)_3$ (**1**). Complex **1** crystallizes in the orthorhombic space group $P2_12_12_1$ with unit cell parameters a = 10.747 (3) Å, b = 12.511 (3) Å, c = 18.897 (4) Å and D_c = 1.31 g cm^{-3} for Z = 4. Least-squares refinement using 2141 independent observed reflections led to a final R value of 0.025. The metal atom is essentially octahedral, and the acyl ligand is coordinated in an η^2 fashion with Mo–C(acyl) = 2.024 (6) Å and Mo–O(acyl) = 2.324 (4) Å. The η^2-acyl linkage in the above complexes remains unchanged upon carbonylation to afford the corresponding $Mo(\eta^2\text{-}COR)X(CO)_2(PMe_3)_2$ derivatives. Similarly, interaction of the $Mo(\eta^2\text{-}COR)X(CO)_n(PMe_3)_{4-n}$ (n = 1,2) complexes with NaS_2CNMe_2 causes loss of one of the trimethylphosphine ligands and formation of new η^2-acyl derivatives $Mo(\eta^2\text{-}COR)(S_2CNMe_2)(CO)_n(PMe_3)_{3-n}$ (n = 1,2). The reaction of **1** with $NaS_2CNMe_2{\cdot}2H_2O$ yields an unprecendented acetyl complex $Mo(COCH_3)(S_2CNMe_2)(CO)(PMe_3)_2$ (**2**), in which the molybdenum atom attains an 18-electron configuration by virtue of a strong interaction with a β-C–H bond of the acetyl group. Complex **2** can also be prepared by reaction of $Mo(\eta^2\text{-}COCH_2SiMe_3)(S_2CNMe_2)(CO)(PMe_3)_2$ with H_2O or by interaction of $Mo(\eta^2\text{-}COCH_3)X(CO)(PMe_3)_3$ (X = Cl,I) with NaS_2CNMe_2 and has been characterized by a complete X-ray structure determination. **2** crystallizes in the monoclinic space group $P2_1/c$ with unit cell parameters a = 11.633 (5) Å, b = 9.962 (4) Å, c = 17.266 (6) Å, β = 95.80 (3)°, and D_c = 1.42 g cm^{-3} for Z = 4. Least-squares refinement based on 1720 independent observed reflections led to a final R value of 0.029. The acyl carbon is bonded to the Mo atom at a Mo–C separation of 2.05 (1) Å, and the acyl methyl group is displaced toward the Mo atom with Mo–C and Mo–H separations of 2.60 (1) and 2.06 (9) Å, respectively.

The carbon monoxide migratory insertion reaction is a key step in many catalytic transformations and as such, and because of its fundamental importance, it has been the subject of a large number of synthetic, mechanistic, and theoretical studies.[1] The generally accepted mechanism for this reaction invokes the intermediacy of a coordinatively unsaturated acyl, whose nature remains unclear. A number of stable transition-metal acyl complexes have been prepared and structurally characterized in recent years, and the acyl group has been found to coordinate to the metal atom in either a monohapto, M–C(O)R, or dihapto, $\overline{M\text{–}C(O)R}$, fashion.[2] In addition, bridging acyl units, η^2 bonded to two or three metal atoms via the acyl C and O atoms, have been also verified.[3] While for some CO insertion reactions the proposed intermediates are formulated as coordinatively unsaturated σ-acyls, i.e., monohapto M–C(O)R species, the existence of an increasing number of compounds in which the acyl group functions formally as a three-electron donor ligand through its C and O atoms seems to support the η^2-acyl formulation proposed for the intermediates in some carbonyl insertion and decarbonylation reactions. Nevertheless, although for the well-known $Mn(CO)(CH_3)$–$Mn(CO\text{-}CH_3)$ system both MO[1f] and mechanistic studies[1c] are neither against nor in favor of an η^2-acetyl structure for the Mn(COC-

† Universidad de Sevilla.
‡ University of Alabama.
§ Northern Illinois University.

(1) (a) Collman, J. P. and Hegedus, L. S. "Principles and Applications of Organotransition Metal Chemistry"; University Science Books: Mill Valley, CA, 1980. (b) Calderazzo, F. *Angew. Chem., Int. Ed. Engl.* **1977**, *16*, 299–311. (c) Flood, T. C.; Jensen, J. E.; Statler, J. A. *J. Am. Chem. Soc.* **1981**, *103*, 4410–4414. (d) Casey, C. P.; Baltusis, L. M. *Ibid.* **1982**, *104*, 6347–6353. (e) Jablonski, C. R.; Wang, Y. *Inorg. Chem.* **1982**, *21*, 4037–4044. (f) Berke, H.; Hoffman, R. *J. Am. Chem. Soc.* **1978**, *100*, 7224–7236.

(2) Churchill, M. R.; Chang, S. W. Y. *Inorg. Chem.* **1975**, *14*, 1680–1716. Fachinetti, G.; Floriani, C.; Marchetti, F.; Merlino, J. *J. Chem. Soc., Chem. Commun.* **1976**, 522–523.

(3) (a) Wong, W.-K.; Wilkinson, G.; Galas, A. M.; Hursthouse, M. B.; Thornton-Pett, M. *J. Chem. Soc., Dalton Trans.* **1981**, 2496–2500. (b) Kampe, C. E.; Boag, N. M.; Kaesz, H. D. *J. Am. Chem. Soc.* **1983**, *105*, 2896–2897. (c) Longato, B.; Norton, J. R.; Huffman, J. C.; Marsella, J. A.; Coulton, K. G. *Ibid.* **1981**, *103*, 209–210.

0002-7863/84/1506-3214$01.50/0